Iraqi Journal of Science, 2024, Vol. 65, No.1, pp: 223- 241
DOI: 10.24996/ijs.2023.65.1.20

ISSN: 0067-2904

# Paleoenvironmental Conditions of the Harur Formation (Early Carboniferous), Northern Iraq: Insights from Mineralogy and Elemental Geochemistry

**Safwan F.H. Al-Lhaebi[1], Flyah H. Al-Khatony[1], Salim H. Hussain[1], Ali I. Al-Juboury*[2], Harry Rowe[3], and Giovanni Zanoni[3]**

*[1]Geology Department, College of Science, University of Mosul, Iraq*
*[2]Petroleum Engineering Department, College of Engineering, Al-Kitab University, Kirkuk, Iraq*
*[3]Premier Corex Laboratories, Houston, TX 77041, USA*

Received: 28/6/2022 Accepted: 25/12/2022 Published: 30/11/2023

**Abstract**

The early Carboniferous Harur Formation from the Ora outcrop section of northern Iraq consists of black shale, calcareous shale and carbonate. The mineralogical and geochemical investigations (major and trace elements) of the black shale and calcareous shale units have been conducted to evaluate paleoenvironmental conditions including paleoclimate, paleoredox conditions, paleoproductivity, sedimentary rate, and to evaluate their effects on organic matter accumulation. The geochemical proxies such as the Chemical Index of Alteration (CIA), A-CN-K plot, Sr/Cu ratio, and the relation between the ratio of Ga/Rb and Sr/Cu suggest moderate to intense chemical weathering under humid conditions. The Rb/K and Sr/Ba ratios indicate a freshwater environment during deposition. Multiple paleo-redox indicators such as ratios of V/(V+Ni) and Th/U) and U index indicates deposition under depleted marine oxygen conditions and consequently recording an Ocean Anoxic Event (OAE). The Th/U ratio indicates that the sedimentary rate at the lower part of the section is less than that of the upper part of the section. The terrigenous clastic input index (Ti and Al) shows that clastic input reduced from the lower to the upper section which implies that the sea level rose first lower to the upper section. Both Al and Ti have positive correlations with TOC (Total Organic Carbon) which reveal that clastic input was advantageous for OM accumulation. The high ratios of (Fe + Mn)/Ti and the presence of nacrite minerals indicate hydrothermal activity during deposition. Hence, the main control factors of OM accumulation in the black shale and calcareous shale of the Harur Formation were terrigenous clastic fluxes, in addition to paleo-redox conditions and hydrothermal activities. On contrary, paleoproductivity proxies play a relatively less significant role in OM accumulation.

**Keywords:** Harur Formation; Paleo-weathering; Terrigenous clastic input; Anoxic event

*Email: alialjubory@yahoo.com

# الظروف البيئية القديمة لتكوين الهارور (الكاربوني المبكر) شمالي العراق، الدلائل المعدنية والجيوكيميائية

صفوان فتحي اللهيبي[1], فليح حسن الخاتوني[1] ، سالم حامد حسين[1]، علي اسماعيل الجبوري[2]*, هاري روي [3], جيوفاني زانوني[3]

[1]قسم الجيولوجي, كلية العلوم, جامعة الموصل, الموصل, العراق

[2]قسم هندسة النفط, كلية الهندسة, جامعة الكتاب, كركوك, العراق

[3]مختبرات شركة بريمير , هيوستن, تكساس, الولايات المتحدة الاميريكية

**الخلاصة**

يتألف تكوين هارور في مقطع اورا من شمالي العراق من السجيل الاسود والسجيل الجيري والصخور الجيرية. تمت الدراسة المعدنية والجيوكيميائية (للعناصر الرئيسية والشحيحة) للسجيل الاسود والسجيل الجيري لتقييم الظروف البيئية القديمة والمتمثلة بالمناخ القديم، ظروف الاكسدة والاختزال القديمة، الانتاجية القديمة، نسبة الترسيب، وتأثير تجمع المواد العضوية. اقترحت الدلائل الجيوكيميائية مثل الدليل الكيميائي للتغير ومخطط الالمنيوم، الكالسيوم+الصوديوم، والبوتاسيوم ونسبة السترونتيوم/النحاس والعلاقة ما بين الكاليوم/الروبيديوم والسترونتيوم / النحاس الى تأثير التجوية الكيميائية الشديدة تحت ظروف رطبة. كما بينت نسبة الكاليوم/الروبيديوم والسترونتيوم / النحاس الى الترسيب في بيئة مياه عذبة، بينما بينت الدلائل لظروف الاكسدة والاختزال القديمة للفناديوم/الفناديوم + النيكل والثوريوم/اليورانيوم ودليل اليورانيوم الى الترسيب في ظروف ناضبة بالاوكسجين وبما يشير الى ظروفنقص الاوكسجين البحرية القديمة. كما بينت دلائل نسبة الثوريوم/اليورانيوم الى ان نسبة الترسيب اقل في الجزء السفلي من التكوين مقارنة بالجزء العلوي، فيما بينت دلائل الترسيب الفتاتي من التيتانيوم والالمنيوم والعلاقة الموجبة مع تجميع المواد العضوية الى قلة التأثير الفتاتي من اسفل التكوين الى اعلاه، مما قد يدل على انخفاض في مستوى سطح البحر في تلك الفترة. بينت النسبة العالية للحديد والمنغنيز/التيتانيوم ووجود معدن الناكرايت الى التأثير الحرمائي.

## 1. Introduction

The geochemical properties of some major and trace elements and their elemental ratios provide important information about the paleoenvironment of deposition. The geochemical characteristics of elements are influenced by several variables such as paleoclimate, biogenic activity, acidity (PH) and tectonic site during deposition [1, 2, 3, 4, 5, 6]. Therefore, using some index elements or their ratios which are susceptible to paleoenvironmental conditions [7]. Numerous studies on this topic (e.g., [8-11]) used the V / (V+Ni) ratio to explore the paleoredox of marine conditions.

The Harur Formation is one of the primary source rocks in Iraq's western desert and amongst the most promising in northern Iraq [12, 13, 14]. However, the use of geochemical features to address its depositional conditions lacks consensus in the literature. This study is the pioneer study that presents a combination of mineralogy, geochemistry of major and trace elements, and TOC data for samples collected from the Ora outcrop section in extreme northern Iraq. The results are used to infer the paleoclimate, paleoredox conditions, paleoproductivity and sedimentary rate, and paleo marine water depth during deposition of the Harur Formation.

## 2. Geologic Setting

The Hercynian orogeny formed an intracratonic basin in the central part of the Arabian Plate in Iraq, Syria, and Turkey in the late Devonian-early Carboniferous; Tectonic Mega Sequence AP4 of Sharland et al [15, 16]. This basin was situated in the southern hemisphere's tropical

and subtropical regions [17]. In Iraq, the basin extends in both subsurface and surface sections from the western part (Western Desert, such as the Akkas-1 and Khleisia-1 wells) to the Ora area in northernmost Iraq (Figure 1). The basin is dominated by mixed siliciclastic-carbonate succession (Kaista, Ora, and Harur formations) and is thought to have been deposited in a subsiding basin with a broad geographic distribution, resembling epicontinental or epeiric seas in a homoclinic ramp [12, 18-20].

The tectonic evolution of the Arabian Plate during the Late Devonian-Early Carboniferous period was interpreted as a period of extension and compression with Hercynian back-arc rifting, inversion, and uplift caused by the subduction of the Paleo-Tethys margin [15]. This was indicated by the presence of Devonian-Carboniferous volcanic and metamorphics in the Kuh-Sefid area of Irans Sanandaj-Sirjan Zone [16]. At that time, the study area was close to the Sanandaj-Sirjan Zone, which suggests that the hydrothermal activity was influenced by this subduction.

The Harur Formation is exposed in the Kaista and Harur areas, near Chalky Village, the Khabour Valley, and the Geli Sinat and Derashish areas northwest of Shiranish in the Amadia district of northern Iraq (Figure 1). This formation has been recorded in the wells Akkas-1, Key Hole KH 5/1, and Khleisia-1, with thicknesses ranging from 85 to 165 m. [21-24]. The Harur Formation was first recognized and described from the Ora fold, Amadia district, of the Iraqi Northern Thrust Zone by Wetzel and Morton, 1952 in [25]. It conformably overlies the Ora Formation while it is unconformably overlain by the late Permian Chia Zairi Formation (Figure 2). This formation's lithology is composed primarily of thin to medium bedded black, calcareous shales, dolomitic limestone, and black micaceous shale in its lower and upper parts. The total thickness of the formation in the type section is about 62 m, while it is about 56 meters in the studied section. The formation was dated based on the fossil record [25, 26, and 16], corresponding to early Carboniferous (Tournaisian) time.

The depositional environment is considered to be marine neritic; mostly reef and fore-reef [26]. Shirwani et al. [27] investigated an outcrop section in Iraq's Northern Thrust Zone and concluded that the Harur Formation was deposited in a shallow marine environment dominated by reefs and reef flanks. Whereas a subsurface study of the middle Paleozoic succession (Pirispiki, Kaista, Ora, Harur, and Raha formations) in several boreholes from the north and northwestern Iraq by [18] suggested that the Harur Formation was deposited in a deep sub-tidal environment and is a continuation of the ramp setting of the Ora Formation. It is thought to mark the end of the overall transgressive late Devonian-early Carboniferous sequence.

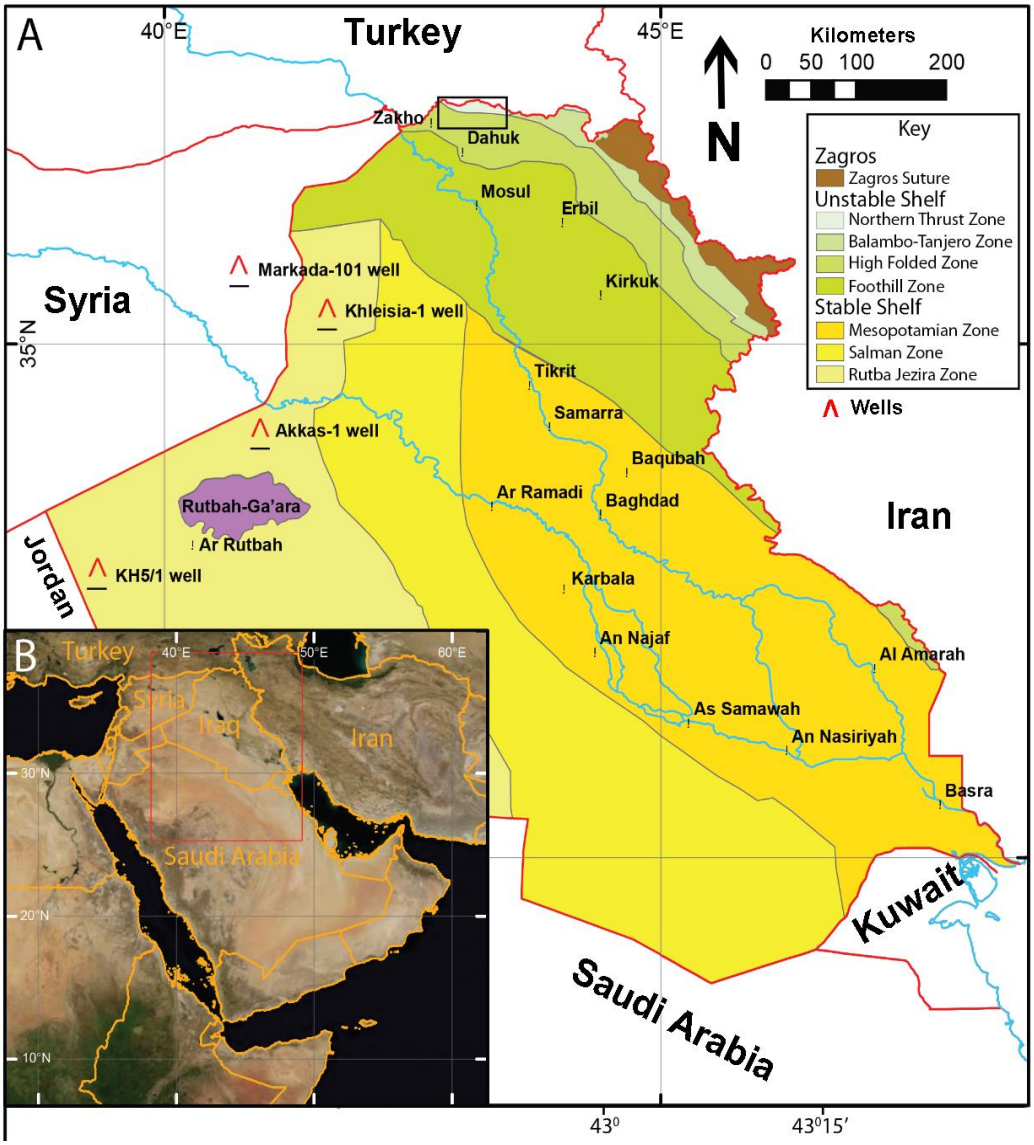


**Figure 1:** A- Iraqi structural map modified after [16, 28] to show the location of wells mentioned in the text. The black box marks the location of the study area in extreme northern Iraq. B-The inset map depicts countries bordering Iraq; the red box indicates the location of map A.

## 3. Materials and Methods

This work was carried out on 12 representative samples from calcareous shales and shale units of the Harur Formation from the exposed northernmost Ora section (Figure 1). These samples were studied for mineralogical compositions through X-Ray Diffraction and Scanner Electron Microscopy (XRD and SEM), analyses of major and trace elements (TEs), as well as Total Organic Carbon (TOC).

The 12 samples for mineralogical examination were subjected to X-ray powder diffraction using a Bruker D8 Advance XRD apparatus at the Premier Oilfield Group Laboratory in Houston, United States. PriBeforeole-rock measurements, the sample was powdered in a McCrone mill for 8 minutes and front-loaded. The measurement parameters were a step scan in the Bragg-Brentano geometry with CuK radiation (40 kV and 40 mA). Sample mounts were scanned from 3 to 70 °2θ at a counting rate of 1.8 s per 0.02 °2θ. The EVA suite and TOPAZ software packages were used to interpret and quantify mineral phases from bulk rock scans.

Scanning electron microscopy observations were performed on six samples to identify the main detrital and diagenetic constituents, particularly those of clay minerals. SEM analyses were performed using a Hitachi S-3000 N Scanning Electron Microscope at the Department of Earth Sciences at Royal Holloway, University of London.

Major and trace elements of 12 samples were identified using the portable Bruker Tracer 5i Energy-Dispersive X-Ray Fluorescence (ED-XRF) spectrometer. Geochemical analyses were also performed at the Premier Laboratory in Houston, Texas, USA.

Twelve samples of shales and intercalated calcareous shales were analyzed for their Total Organic Carbon (TOC) content using a LECO C230 instrument, which requires adopting decarbonization of the rock sample with concentrated hydrochloric acid for two hours. Following that, distilled water was used to remove the treated HCl, and the samples were oven-dried at 110 C° for 4 hours. The samples were then weighed to determine the carbonate percent value based on weight loss. The LECO instrument is calibrated with a standard of known carbon values to check the variation and calibration of the analysis and to verify the data. TOC has an acceptable standard deviation of 3% from the known value. Then, the samples were analyzed using a Wildcat Technologies HAWK pyrolysis instrument to determine organic carbon oxide yields, and the total organic carbon content was calculated using the volume of generated $CO_2$.

## 4. Results

### 4.1. Mineralogical study

#### 4.1.1. XRD analysis

Mineral compositions of the studied samples from XRD analyses have revealed that they are primarily composed of clay minerals represented by mixed layered illite/smectite (I/S) (21.3%) followed by varying amounts of illite/mica (I/M) (17.7%), kaolinite (3.3%), nacrite (2.9%) and chlorite (2.5 %). By contrast, the non-clay mineral assemblages are dominated by quartz (33.0%), carbonate (calcite, 15.5%), dolomite (1.2%), g

goethite (8.1%), k-feldspars (2.2%), plagioclase (1.6 %) and anatase (0.7%) (Figure 3, Table 1). The main carbonate mineral phases are calcite and minor Fe-rich dolomite (ankerite). However, calcite is not uniformly distributed throughout the shale units ($CaCO_3$ 0.5– 75.4 %, avg.= 15.5).

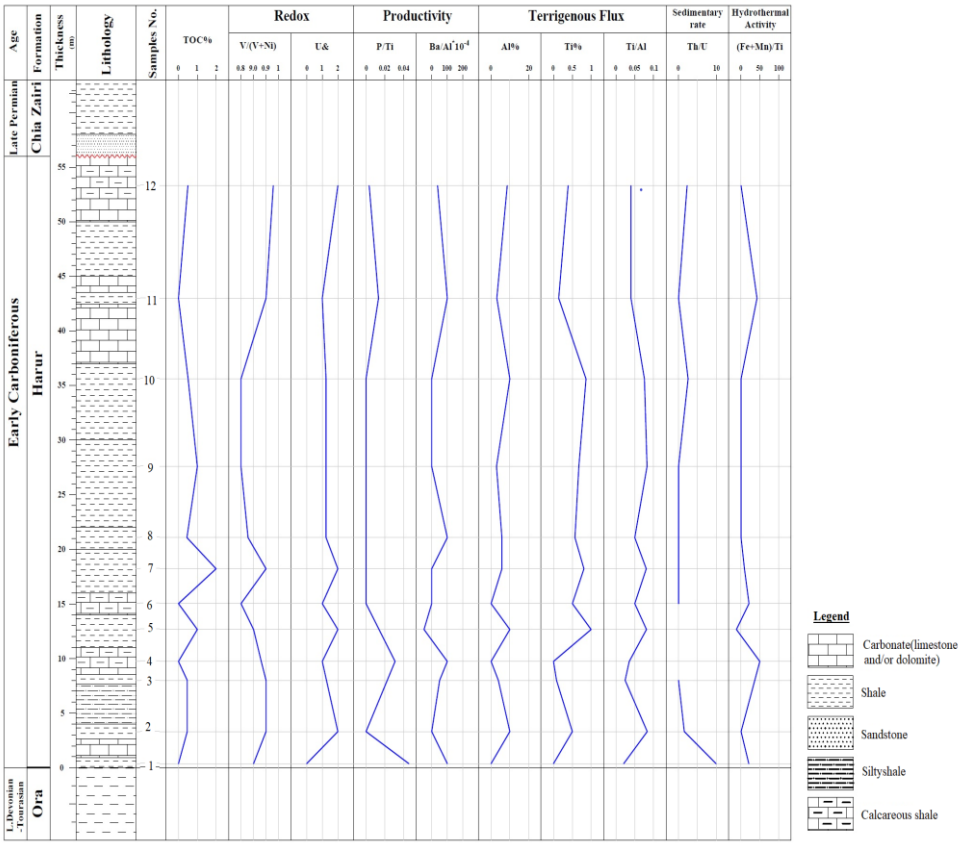


**Figure 2:** Lithological section of the Harur Formation in northern Iraq, with sample locations and geochemical parameters indicating paleoenvironmental conditions.

**Table 1:** Mineral composition (%) of selected samples from the Harur Formation.

| ID | Quartz | K-spar | Plagioclase | Calcite | Fe Dolomite | Chlorite | Illite/Mica | I/S | Kaolinite | Nacrite | Anatase | Goethite |
|---|---|---|---|---|---|---|---|---|---|---|---|---|
| **Har 12** | 19.4 | | | 28.9 | | 2.0 | 23.5 | 20.2 | | | 0.7 | 5.4 |
| **Har 11** | 27.0 | | | 30.4 | | | 12.4 | 10.4 | | 4.4 | 0.4 | 11.9 |
| **Har 10** | 20.8 | 3.6 | 0.3 | 1.1 | 1.6 | | 28.4 | 35.6 | | | 1.0 | 7.6 |
| **Har 9** | 33.4 | 2.3 | 1.1 | | 0.9 | | 23.9 | 18.6 | | 3.6 | 0.9 | 10 |
| **Har 8** | 29.1 | 3.2 | 0.3 | 0.6 | 1.5 | | 26.9 | 26 | | 1.9 | 0.8 | 6.7 |
| **Har 7** | 29.6 | 3.4 | 0.5 | 0.5 | 1.5 | | 25.6 | 24.4 | | 1.8 | 0.7 | 8.5 |
| **Har 6** | 37.2 | 1.1 | | 0.5 | 1.1 | 2.9 | 17.6 | 25.6 | 4.5 | | 0.8 | 8.7 |
| **Har 5** | 30.1 | 3.6 | | 0.7 | 0.8 | | 26.6 | 30.8 | | | 0.9 | 6.6 |
| **Har 4** | 62.1 | 0.5 | 3.5 | | | 3.2 | 0.4 | 17.1 | 3.8 | | | 9.4 |
| **Har 3** | 49.6 | 0.4 | 3.7 | 15.6 | | 3.7 | 4.00 | 15.5 | 1.6 | | 0.5 | 5.5 |
| **Har 2** | 42.7 | 1.8 | | 0.8 | | | 16.8 | 28.4 | | | 0.7 | 8.7 |
| **Har 1** | 14.4 | | | 75.4 | | 0.8 | 5.8 | 3.2 | | | | |
| **Avg.** | 33.0 | 2.2 | 1.6 | 15.5 | 1.2 | 2.5 | 17.7 | 21.3 | 3.3 | 2.9 | 0.7 | 8.1 |
| **Max** | 62.1 | 3.6 | 3.7 | 75.4 | 1.6 | 3.7 | 28.4 | 35.6 | 4.5 | 4.4 | 1.0 | 11.9 |
| **Min** | 14.4 | 0.4 | 0.3 | 0.5 | 0.8 | 0.8 | 0.4 | 3.2 | 1.6 | 1.8 | 0.4 | 5.4 |

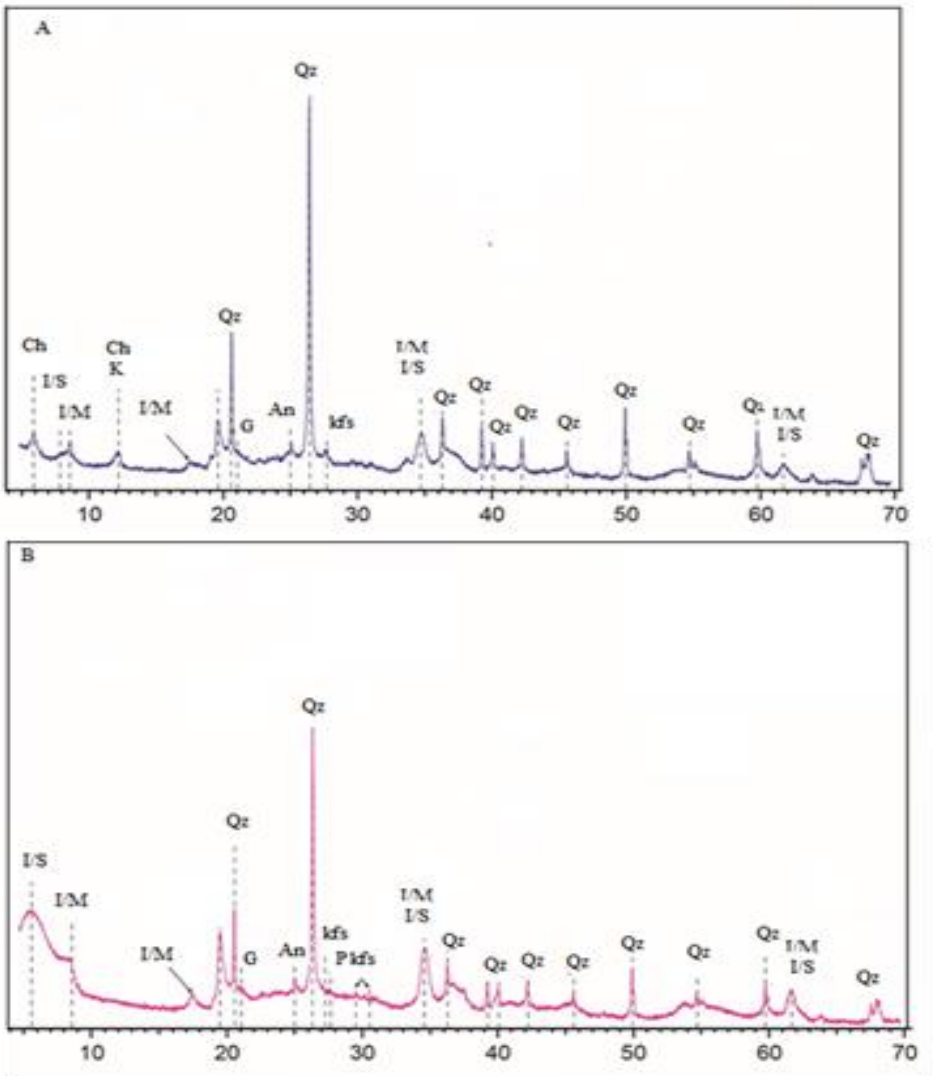


**Figure 3 :** Representative X-ray diffractograms of the main clay and non-clay mineral components in the studied shales. I/S=Illite/Smectite; I/M=Illite/Mica, Qz=Quartz, kfs=K-Feldspar, G=Goethite, An=Anatase, P=Plagioclase, K=Kaolinite, and Ch=Chlorite. Quantitative mineral content is found using the EVA suite and TOPAZ software.

### 4.1.2. SEM analysis

Scanning electron microscopic analysis shows that the shale is mostly composed of illite/smectite (I/S) and detrital illite/mica (I/M) in the form of irregular interlocking flakes. (Figure 4a). Illite/smectite is commonly found in the form of webby or honeycomb morphology, whereas Figure 4b displays the kaolinite absence. Detrital mica plates are often present and associated with I/S (Figure 4b and c). Non-clay minerals are dominated by detrital carbonate (calcite with few dolomites) and quartz which occur as fine grains and/or lumps either filling fractures and pore space or distributed randomly throughout the matrix (Figure 4d). Fractures and vugs/pores are commonly present in the studied samples (Figure 4 a-d).

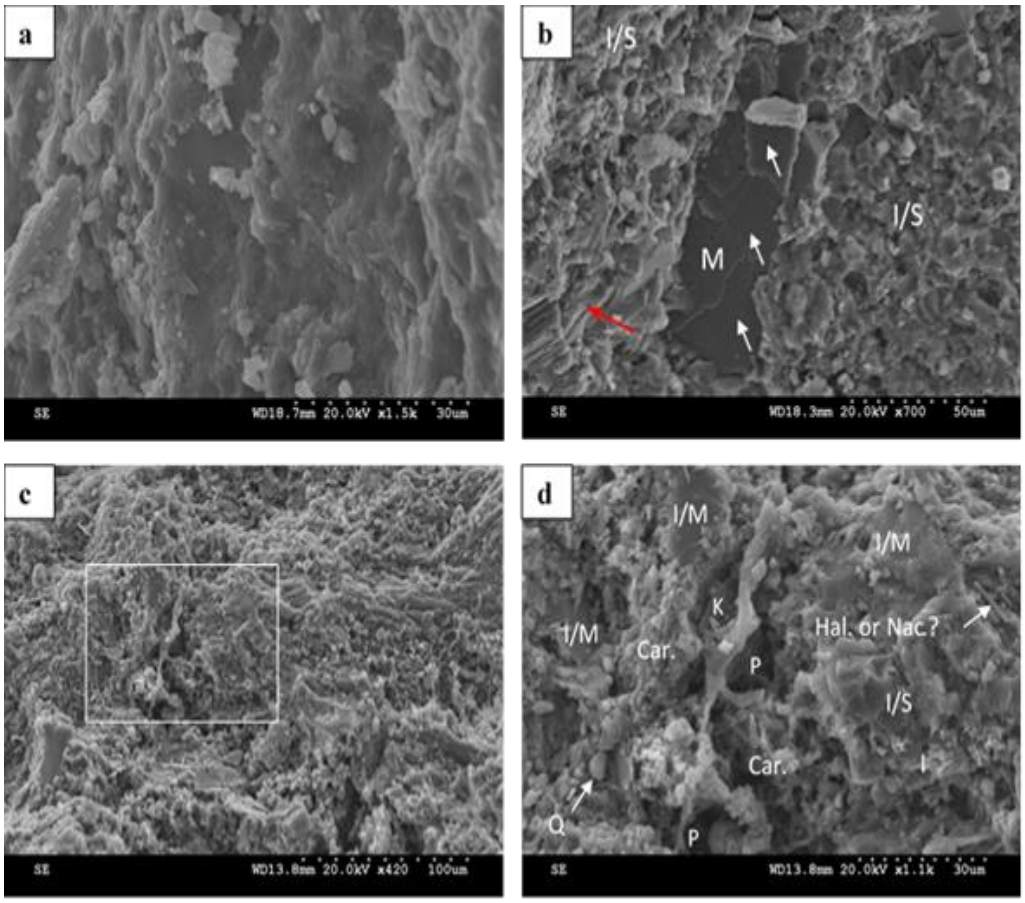


**Figure 4 :** Scanning electron micrographs of Harur shales. a) Matted sheets of irregular, ragged detrital illite/smectite oriented parallel to each other (Har1). b) honeycomb and flaky illite-smectite mixed layer associated with detrital mica (M), note micropores (arrows) in mica plates and booklet-like kaolinite grains (red arrow) (Har10). c) Poorly developed detrital illite/smectite (I/S) and illite/mica (I/M) (Har8). d) Enlarged area of white rectangle in c showing mixed-layer I/S aggregate replaced by fibrous illite (I), illite/mica (I/M), carbonate (Car.), quartz (Q), kaolinite (K), pores (P) and possible halloysite or nacrite? (Hal., Nac).

### 4.2. Geochemistry

#### 4.2.1. Major elements

The average concentration of Major Element Oxides (MEO) is dominated by $SiO_2$ (44.14%), followed by $Al_2O_3$ (15.11%), $Fe_2O_3$ (9.40 %), CaO (8.55%), $K_2O$ (2.60%), and MgO (1.82%). Other MEO fall below 1.0%, which include $TiO_2$ (0.86%), $Na_2O$ (0.58%), P2O5 (0.07%), and MnO (0.03%). According to a cross plot of Log ($Fe_2O_3/K_2O$) versus Log ($SiO_2/Al_2O_3$), most of the studied samples are classified as Fe-shale and shale (Figure 5).

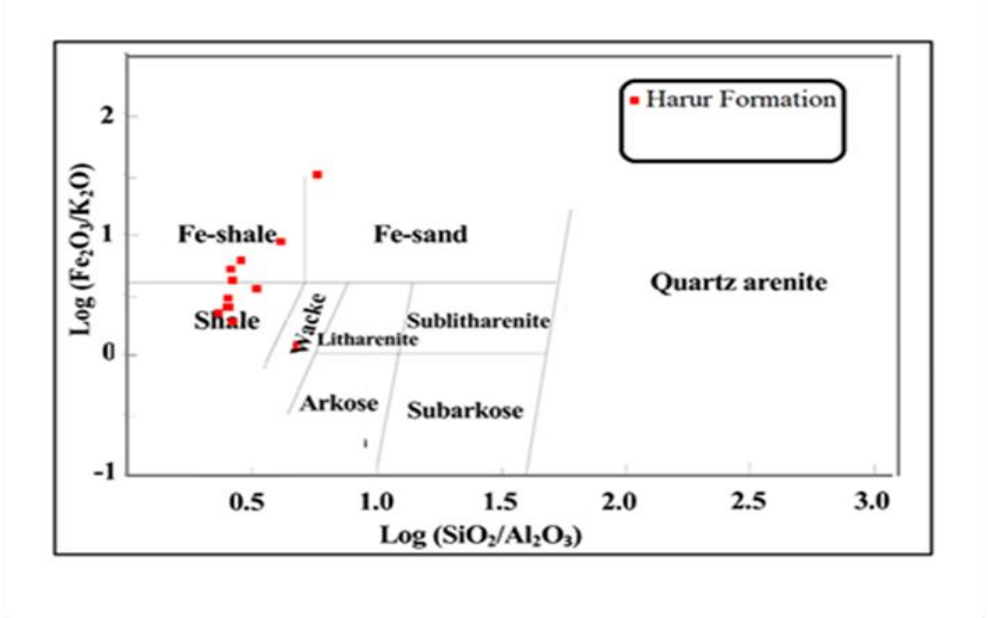


**Figure 5:** Geochemical classification of siliciclastic sediments of Harur shales (after [29]).

### 4.2.2. Trace elements

The concentration of trace elements (TEs) for the Harur Formation as presented in Table 2 shows that the most abundant TEs in their average concentrations are Mn (450.01ppm) Ba (417.11 ppm), V (220.51ppm), Zr (187.69ppm), Cr (106.77ppm), Sr (101.82 ppm), Rb (89.60ppm), Zn (88.00ppm), Ni (38.81ppm), and Cu (23.25 ppm). The other TEs are lower than 10ppm, which include U (7.46ppm), Mo (5.78ppm), Th (5.60ppm) and Co (3.07ppm (Table 2).

The enrichment factor (EF) has been widely used to characterize the degree of enrichment in different clastic sediments by normalizing each element to aluminium (Al) and comparing their normalization ratios to the upper continental crust (UCC; [30]). The average enriched TEs (EF > 1) of the studied samples mainly include Mo (3.89), U (2.55), V (2.33), Zn (1.41), Ga (1.37), Co (1.31), Cr (1.30), Cu (1.12), Zr (1.00) and Pb (1.00) (Table 2). Conversely, the depleted TEs (EF < 1) are composed of Ni (0.98), Ba (0.87), Rb (0.84), Sr (0.73), and Th (0.57), (Figure 6).

### 4.2.3. Total Organic Carbon (TOC)

TOC contents in shales and calcareous shale samples are presented in Table 2 and Figure 2. TOC values vary from 0.12 to 1.43 wt. %, with a mean value of 0.4 wt. %. Lower values of TOC less than 1% wt. % were found in ten samples, while higher values of more than 1% wt. % were found in two samples (Har7 and Har9). The TOC contents, on the other hand, vary throughout the section, with higher values in the middle and lower values in the lower and upper parts (Figure 2).

**Table 2 :** TOC and major-element oxide concentrations (in weight%), as well as the Chemical Index of Alteration (CIA).

| Sample No. | TOC | $SiO_2$ | $Al_2O_3$ | $TiO_2$ | $Fe_2O_3$ | MnO | MgO | CaO | $K_2O$ | $Na_2O$ | $P_2O_5$ | CIA |
|---|---|---|---|---|---|---|---|---|---|---|---|---|
| Har 12 | 0.31 | 39.64 | 14.97 | 0.54 | 6.55 | 0.03 | 1.93 | 17.91 | 3.52 | 0.06 | 0.09 | 97.56 |
| Har 11 | 0.24 | 32.57 | 11.38 | 0.43 | 10.07 | 0.03 | 1.61 | 21.72 | 1.67 | 0.69 | 0.14 | 91.35 |
| Har 10 | 0.89 | 49.66 | 21.38 | 1.40 | 9.40 | 0.03 | 2.01 | 1.04 | 4.33 | 0.42 | 0.00 | 98.00 |
| Har 9 | 1.14 | 47.22 | 17.84 | 1.28 | 11.55 | 0.03 | 1.85 | 1.41 | 2.83 | 0.77 | 0.00 | 95.74 |

| | | | | | | | | | | | | |
|---|---|---|---|---|---|---|---|---|---|---|---|---|
| Har 8 | 0.89 | 50.74 | 19.79 | 1.19 | 9.28 | 0.03 | 1.90 | 1.11 | 3.77 | 0.65 | 0.00 | 96.73 |
| Har 7 | 1.43 | 49.52 | 19.49 | 1.36 | 10.04 | 0.03 | 1.82 | 1.06 | 3.44 | 0.70 | 0.00 | 96.46 |
| Har 6 | 0.44 | 46.66 | 17.87 | 1.05 | 12.29 | 0.03 | 2.13 | 1.29 | 2.42 | 0.97 | 0.00 | 94.76 |
| Har 5 | 0.91 | 50.57 | 20.05 | 1.36 | 9.29 | 0.03 | 1.80 | 1.14 | 3.78 | 0.73 | 0.01 | 96.39 |
| Har 4 | 0.28 | 48.09 | 8.34 | 0.29 | 13.70 | 0.03 | 2.35 | 1.95 | 0.44 | 0.55 | 0.22 | 93.47 |
| Har 3 | 0.53 | 43.36 | 10.51 | 0.33 | 9.96 | 0.03 | 1.97 | 13.08 | 1.16 | 0.84 | 0.17 | 90.75 |
| Har 2 | 0.59 | 52.15 | 15.69 | 0.98 | 9.32 | 0.03 | 1.60 | 2.00 | 2.67 | 0.44 | 0.00 | 97.04 |
| Har 1 | 0.43 | 19.48 | 4.01 | 0.11 | 1.40 | 0.03 | 0.85 | 38.93 | 1.18 | 0.14 | 0.18 | 82.81 |
| Ave | 0.67 | 44.14 | 15.11 | 0.86 | 9.40 | 0.03 | 1.82 | 8.55 | 2.60 | 0.58 | 0.07 | 94.26 |
| Max | 1.43 | 52.15 | 21.38 | 1.40 | 13.70 | 0.03 | 2.35 | 38.93 | 4.33 | 0.97 | 0.22 | 98.00 |
| Min | 0.24 | 19.48 | 4.01 | 0.11 | 1.40 | 0.03 | 0.85 | 1.04 | 0.44 | 0.06 | 0.00 | 82.81 |

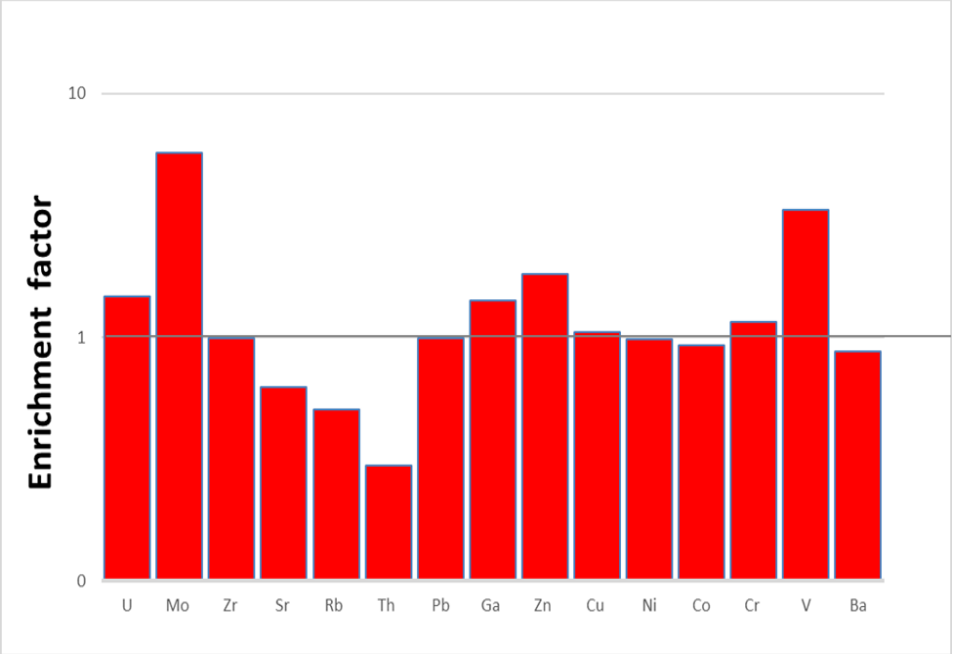


**Figure 6 :** EFs diagram of the Harur Formation's selected trace elements. An element enrichment or depletion is indicated by a horizontal line (EF = 1).

**Table 3:** Trace elements (in ppm) and elemental ratios sensitive to environmental conditions of the study samples for the Harur Formation.

| Sample No. | Co | Ni | Cu | Zn | Ga | Pb | Th | Rb | Sr | Zr | Mo | U- | Cr | V | Ba |
|---|---|---|---|---|---|---|---|---|---|---|---|---|---|---|---|
| Har 12 | 15.88 | 28.46 | 14.14 | 29.02 | 24.23 | 15.88 | 7.97 | 129.05 | 82.23 | 169.54 | 6.23 | 4.20 | 103.25 | 285.65 | 359.77 |
| Har 11 | 11.76 | 36.33 | 19.67 | 96.95 | 18.05 | 12.58 | 2.38 | 42.33 | 164.26 | 141.42 | 6.42 | 3.09 | 72.09 | 267.29 | 391.36 |
| Har 10 | 0.00 | 41.19 | 30.02 | 56.52 | 33.39 | 12.97 | 11.20 | 176.36 | 0.00 | 215.48 | 7.90 | 5.81 | 148.51 | 188.28 | 367.45 |
| Har 9 | 0.00 | 47.43 | 19.56 | 81.38 | 29.69 | 13.81 | 5.21 | 86.55 | 16.31 | 222.64 | 5.61 | 12.52 | 136.19 | 215.24 | 333.26 |
| Har 8 | 0.00 | 40.25 | 26.29 | 69.40 | 31.21 | 14.62 | 8.08 | 128.93 | 37.60 | 224.41 | 3.72 | 13.24 | 143.19 | 187.65 | 988.99 |
| Har 7 | 0.00 | 41.80 | 14.55 | 151.22 | 27.39 | 14.62 | 7.37 | 117.57 | 50.48 | 301.64 | 11.00 | 12.14 | 144.41 | 205.95 | 388.52 |
| Har 6 | 0.00 | 48.12 | 34.07 | 86.88 | 26.49 | 13.78 | 4.35 | 73.49 | 41.44 | 228.00 | 6.74 | 8.96 | 116.75 | 276.26 | 394.09 |
| Har 5 | 0.00 | 42.48 | 19.26 | 86.02 | 31.44 | 15.10 | 8.78 | 140.24 | 25.73 | 227.77 | 7.12 | 12.94 | 146.74 | 194.35 | 192.58 |
| Har 4 | 0.00 | 46.28 | 35.18 | 187.91 | 14.44 | 18.81 | 0.00 | 0.00 | 175.30 | 116.98 | 3.25 | 7.01 | 48.22 | 260.35 | 425.10 |
| Har 3 | 0.00 | 39.67 | 33.35 | 90.81 | 14.79 | 11.92 | 1.46 | 24.25 | 109.28 | 242.31 | 7.30 | 4.98 | 59.52 | 248.58 | 398.31 |
| Har 2 | 0.00 | 38.95 | 19.78 | 107.94 | 27.81 | 15.83 | 7.45 | 120.17 | 22.01 | 134.26 | 3.44 | 4.22 | 122.79 | 243.69 | 521.44 |

| | | | | | | | | | | | | | | | |
|---|---|---|---|---|---|---|---|---|---|---|---|---|---|---|---|
| **Har 1** | 9.15 | 14.81 | 13.09 | 11.93 | 4.18 | 9.97 | 3.00 | 36.31 | 497.19 | 27.81 | 0.60 | 0.36 | 39.56 | 72.81 | 244.43 |
| **Avg.** | 3.07 | 38.81 | 23.25 | 88.00 | 23.59 | 14.16 | 5.60 | 89.60 | 101.82 | 187.69 | 5.78 | 7.46 | 106.77 | 220.51 | 417.11 |
| **Max** | 15.88 | 48.12 | 35.18 | 187.91 | 33.39 | 18.81 | 11.20 | 176.36 | 497.19 | 301.64 | 11.00 | 13.24 | 148.51 | 285.65 | 988.99 |
| **Min** | 0.00 | 14.81 | 13.09 | 11.93 | 4.18 | 9.97 | 0.00 | 0.00 | 0.00 | 27.81 | 0.60 | 0.36 | 39.56 | 72.81 | 192.58 |

**Table 3, Continued**

| Sample No. | V/(V+Ni) | Cu/Zn | δU | V/Cr | Ga/Rb | Sr/Cu | Sr/Ba | Rb/K | U/Th | P/Ti | P/Al | Ba/Al | Ba/Sr | Th/U | Ti/A1 |
|---|---|---|---|---|---|---|---|---|---|---|---|---|---|---|---|
| **Har 12** | 0.91 | 0.49 | 1.22 | 2.77 | 0.19 | 5.81 | 0.23 | 0.004 | 0.53 | 0.124 | 0.01 | 45.40 | 4.38 | 1.90 | 0.04 |
| **Har 11** | 0.88 | 0.20 | 1.59 | 3.71 | 0.43 | 8.35 | 0.42 | 0.003 | 1.30 | 0.238 | 0.01 | 64.98 | 2.38 | 0.77 | 0.04 |
| **Har 10** | 0.82 | 0.53 | 1.22 | 1.27 | 0.19 | | | 0.005 | 0.52 | | | 32.48 | | 1.93 | 0.07 |
| **Har 9** | 0.82 | 0.24 | 1.76 | 1.58 | 0.34 | 0.83 | 0.05 | 0.004 | 2.40 | | | 35.29 | 20.43 | 0.42 | 0.08 |
| **Har 8** | 0.82 | 0.38 | 1.66 | 1.31 | 0.24 | 1.43 | 0.04 | 0.004 | 1.64 | 0.002 | 0.00 | 94.42 | 26.30 | 0.61 | 0.07 |
| **Har 7** | 0.83 | 0.10 | 1.66 | 1.43 | 0.23 | 3.47 | 0.13 | 0.004 | 1.65 | | | 37.67 | 7.70 | 0.61 | 0.08 |
| **Har 6** | 0.85 | 0.39 | 1.72 | 2.37 | 0.36 | 1.22 | 0.11 | 0.004 | 2.06 | | | 41.67 | 9.51 | 0.49 | 0.07 |
| **Har 5** | 0.82 | 0.22 | 1.63 | 1.32 | 0.22 | 1.34 | 0.13 | 0.004 | 1.47 | 0.006 | 0.00 | 18.15 | 7.49 | 0.68 | 0.08 |
| **Har 4** | 0.85 | 0.19 | 2.00 | 5.40 | | 4.98 | 0.41 | | | 0.537 | 0.02 | 96.33 | 2.43 | | 0.04 |
| **Har 3** | 0.86 | 0.37 | 1.82 | 4.18 | 0.61 | 3.28 | 0.27 | 0.003 | 3.41 | 0.371 | 0.01 | 71.64 | 3.64 | 0.29 | 0.04 |
| **Har 2** | 0.86 | 0.18 | 1.26 | 1.98 | 0.23 | 1.11 | 0.04 | 0.005 | 0.57 | | | 62.81 | 23.70 | 1.76 | 0.07 |
| **Har 1** | 0.83 | 1.10 | 0.53 | 1.84 | 0.12 | | 2.03 | 0.004 | 0.12 | 1.195 | 0.04 | 115.6 | 0.49 | 8.22 | 0.03 |
| **Avg.** | 0.85 | 0.37 | 1.51 | 2.43 | 0.29 | 3.18 | 0.35 | 0.004 | 1.42 | 0.35 | 0.02 | 59.70 | 9.86 | 1.61 | 0.06 |
| **Max** | 0.91 | 1.1 | 2 | 5.4 | 0.61 | 8.35 | 2.03 | 0.005 | 3.41 | 1.195 | 0.04 | 115.6 | 26.3 | 8.22 | 0.08 |
| **Min** | 0.82 | 0.1 | 0.53 | 1.27 | 0.12 | 0.83 | 0.04 | 0.003 | 0.12 | 0.002 | 0.01 | 18.15 | 0.49 | 0.29 | 0.03 |

## 5. Discussion

### 5.1. Paleoenvironmental conditions

#### 5.1.1. Paleoclimate and salinity

The paleoclimate of the sediments is traditionally reconstructed using the Chemical Index of Alteration (CIA= [$Al_2O_3$/ ($Al_2O_3$ + CaO* + $Na_2O$ + $K_2O$)] × 100; [31] and to assess the parent rock's degree of weathering [32]. The CIA is calculated as CIA= [($Al_2O_3$)/($Al_2O_3$+CaO*+ $Na_2O$ + $K_2O$)]100, where $Al_2O_3$, CaO, $Na_2O$, and $K_2O$ are in molar proportions and CaO* is calcium derived from silicate minerals [30]. In this study, we use the method of McLennan et al. [33] to obtain CaO*. If the CaO value after apatite correction [molar CaO (corrected) = molar CaO-(10/3 molar $P_2O_5$)] is greater than $Na_2O$, the CaO* is accepted as $Na_2O$. Otherwise, the CaO* value is assumed to be the same as the CaO value.

The CIA values of the study samples range from 82.81 to 98.00 (avg.94.26; Table 2), indicating a moderate to a high degree of chemical weathering.

The A-CN-K diagram can also be used to restore the paleo-weathering condition ([34]; Figure 7). The studied samples are located above the K-feldspar-plagioclase line, parallel to the A-K join, and close to the illite point in this plot, indicating moderate to intense chemical weathering under humid conditions.

The Sr/Cu ratio is another common proxy for paleoclimate studies, and a higher ratio indicates a dry paleoclimate condition [35]. According to these authors, Sr/Cu ratios between 1.3 and 5 indicate a humid climate, whereas Sr/Cu ratios greater than 5 indicate a dry and hot climate. The Sr/Cu ratios of the studied samples range from 0.83 to 8.35 (avg. =3.18) and are less than 5, indicating that the Harur Formation was deposited under humid climatic conditions, as shown in Table 3. Moreover, the cross plot of the Ga/Rb versus Sr/Cu ratio indicates that the majority of the studied samples fall on a warm humid field (Figure 8).

The type of clay minerals can also reflect the palaeoclimate. The clay mineral assemblage of the shale samples (Table 1) is dominated by illite/smectite, as revealed by SEM analysis. The high illite/smectite ratio, combined with illite/mica, and chlorite (Table 1, Figure 4) indicate intense chemical weathering under warm and humid climatic conditions [36].

Furthermore, kaolinite is an excellent predictor of a humid climate, whereas smectite and smectite mixed layers are byproducts of a warm, moist climate [35]. Chlorite, on the other hand, does not typically survive in cool, moist environments, its presence in sediments as a detrital clay is a good indicator of cool/dry climates [37, 38].

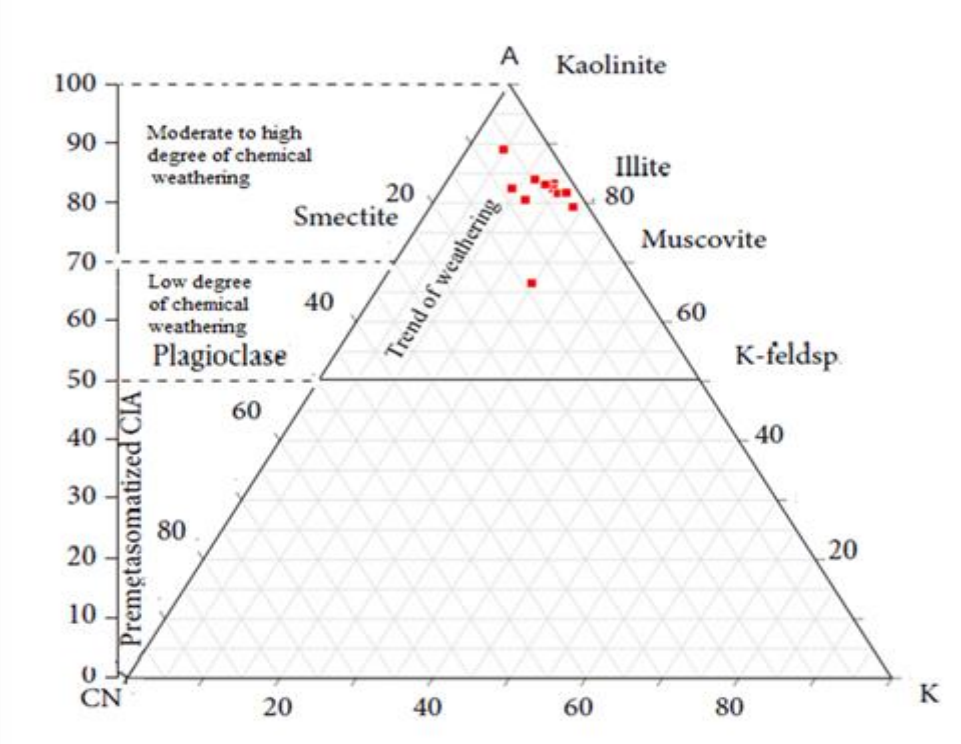


**Figure 7:** Ternary plot ACNK [$Al_2O_3$ - (CaO*+$Na_2O$) - $K_2O$; all in molar proportions] for the Harur Formation (After [31, 34]).

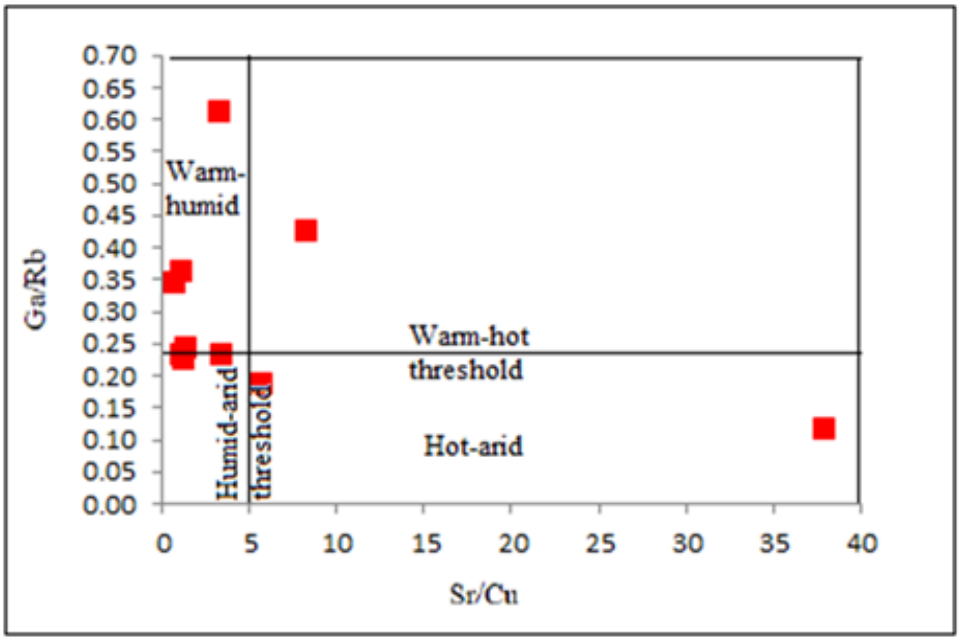


**Figure 8 :** A cross plot of the Ga/Rb versus Sr/Cu ratio suggests primarily a warm-humid climate (after [35]).

All of the data presented above is consistent with the Devonian-early Carboniferous paleoclimate of the broad shelf depositional basin, including the Harur Formation in Iraq, which was located between tropical and subtropical southern hemispheres [14].
The ratios of Rb/K [39] and Sr/Ba [39] can be used to assess paleosalinity conditions during deposition (e.g., [40, 41]). Rb/K ratios of ≤ 0.004 reveal freshwater column, 0.004 ≤ 0.006 denotes a fresh to the brackish water environment, and >0.006 values indicate fully marine water conditions. Sr/Ba ratios greater than one indicate saline water conditions, 1.0 to 0.6 indicate brackish water conditions, and less than 0.6 indicates freshwater conditions [40, 41]. The Rb/K ratios of the studied samples range from 0.003 to 0.005 (avg. 0.004), which is typical of freshwater conditions. Similarly, the Sr/Ba ratios range from 0.04 to 2.03 (avg. 0.35) (Table 3), indicating a freshwater environment during deposition.

### 5.1.2. Paleoredox conditions

Trace elements in sediments such as V, Ni, U, and Mo are more sensitive to environmental changes than other elements and have been widely used to infer paleoredox conditions of water due to their insolubility in reducing environments and being more enriched under anoxic marine conditions [ 8, 9, 42, 11]. The V/(V+Ni) ratio is a useful proxy for palaeo-redox reconstruction because it consistently indicates lower oxygen regimes than other paleoredox indicators [10]. Hatch and Leventhal [8] proposed V/(V+Ni) ratios ranging from 0.46-0.60 in dysoxic environments to 0.54-0.82 in anoxic environments and up to 0.84 in euxinic environments. The V/(V+Ni) ratios of the shale samples in this study range from 0.82 to 0.91 (avg. = 0.85). (Table 3). These values all point to deposition under anoxic conditions.
The Th/U ratio is also used as a redox indicator, with ratios ranging from 0 to 2 indicating a reducing environment, 2 to 7 denoting an oxic environment, and > 8 implying a strongly oxidizing environment [43]. The Th/U ratios of the shale samples range from 0.3 to 8.2 (avg. = 1.6), indicating anoxic conditions. The U index [&U = U⁄¬0.5 × (Th⁄3 + U)] is another proxy for reconstructing paleoredox conditions, with a value greater than one indicating a reducing environment and a value less than one indicating an oxidizing environment [44]. The U index

values of the Harur shale vary from 0.5 to 2.0 (avg. = 1.5) (Table 3), indicating an anoxic condition, as do the other indicators.

### 5.1.3. Paleoproductivity

Many geochemical proxies, including phosphorus and barium, have been used to assess the role of paleoproductivity in the formation of organic-rich rocks [45, 46]. Phosphorus (P) and barium (Ba) are the two most abundant elements in skeletal material and play critical roles in metabolic processes [47-49]. The P/Ti and Ba/Al ratios are commonly employed because they ignore the effect of detrital input [50, 51].

The P/Ti and Ba/Al ratios of the Harur shale range from 0.00 to 0.04 (avg. 0.01) and 18.15*10-4 to 115.26 *10-4 (avg. 59.67*10-4) respectively (Table 3; Fig. 2). These ratios are significantly less than the lower productivity value of P/Ti (0.34) and Ba/Al (34*10-4) respectively. Moreover, these ratios have a weak correlation with the TOC (R2 =-0.3 and -0.2 respectively) (Figure 9). These data may indicate that productivity is less significant in organic matter accumulation.

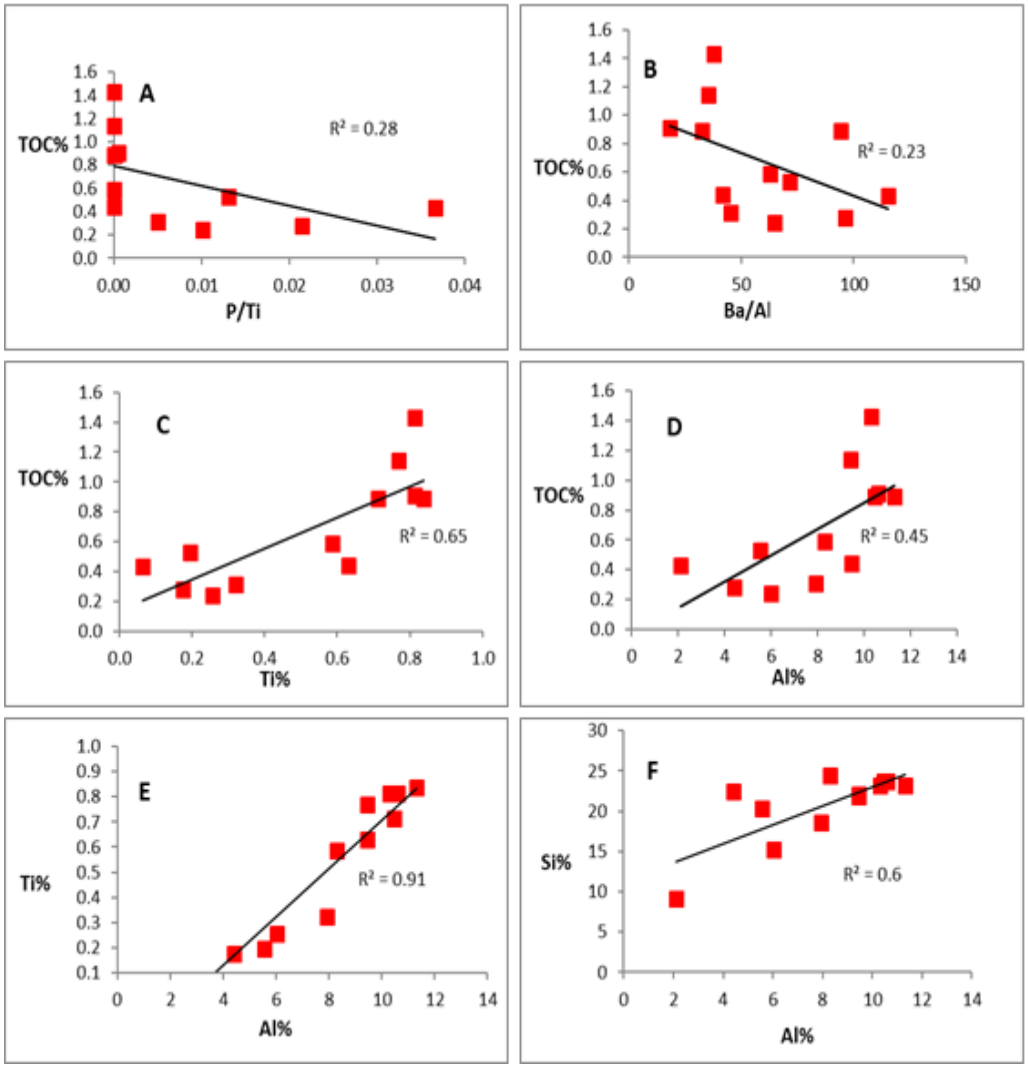


**Figure 9 :** Correlation coefficients (A-D) between TOC with (A) P/Ti, (B) Ba/Al, (C) Ti and (D) Al, and (E and F) between Al with both Ti and Si.

### 5.1.4. Terrigenous clastic input and sedimentary rate

Aluminium and titanium elements have been considered indicators of detrital flux since they are commonly immobile during diagenesis [52-54]. However, these elements can only be used when there is a positive correlation between Al and Ti because they may be influenced by other factors independent of terrestrial flux, such as pH and authigenic clay minerals [55, 56, 54]. The results of the present study demonstrate that Al and Ti have similar curve patterns (Figure 2) and they display a strong positive correlation (R2 = 0.91; Figure 8) suggesting that they are mainly sourced from terrigenous detrital. Furthermore, $Al_2O_3$ has a positive correlation with $SiO_2$ (R2= +0.58), indicating that Si is mostly present as aluminosilicate rather than quartz. Thus, the source of aluminosilicate could be inferred as continental flux.

A mineralogical analysis of the study samples reveals the presence of quartz, clay minerals, feldspars, goethite, and anatase (Figure 3 and Table 1). These minerals may indicate the contribution of detrital input and support geochemical parameters. Iron can be found in the structure of clay minerals or goethite. According to Sharma [57], in the marine environment, iron hydroxides are carried as particles and colloids in suspension and thus tend to aggregate in the fine fraction of sediments. Anatase is typically found as discrete minerals within clays [58]. Ti has a strong positive correlation with Al (R2 =0.9) (Figure 8), indicating that Ti is primarily associated with clays and reflects its terrigenous origin.

Detrital flux depends on the relative sea level, which shifts the site of sedimentation landward during transgression and basinward during regression [52]. Al and Ti generally exhibit decreasing trends from the lower toward the upper section (Figure 2) suggesting that sea-level rise may be due to subsidence and/or transgression.

Organic matter is mainly sourced from two parts, it is partly provided by terrigenous clastic input and the biological productivity in marine environments [59]. The terrigenous clastic influx influences OM accumulation in marine sediments by diluting the OM or providing sites for OM adsorption on clay minerals [60-64; 53]. As a consequence, more than 80% of sedimentary terrigenous OM delivered to the ocean is buried near continental borders at a rate 8 to 30 times greater than in open oceans [65].

Both Al and Ti have positive correlations with TOC (Fig. 8), (R2 =0.5 and 0.7 respectively). In addition, the TOC trend pattern decreases from the lower to the upper part of the studied section and it is nearly identical to the Ti/Al curve (Figure 2). This may reveal that clastic input plays a major role in OM accumulation.

The Ti/A1 ratio is a good predictor of siliciclastic grain size and, consequently, sedimentation rate [66, 67]. Thus, because Al occurs primarily in clay minerals, whereas Ti occurs in both clays and sand- and silt-sized grains such as quartz, augite, sphene and ilmenite, higher Ti/A1 values represent larger grains [61]. The Ti/Al ratios in the studied section ranged between 0.03 and 0.08 (avg. 0.06), and the curve trend does not entirely match the TOC curve (Figure 2). These average values suggest that the grain sizes have a minor effect on OM distribution.

The Th/U ratio can be used as an indicator of sedimentary rate, and higher Th/U values generally indicate a higher sedimentary rate [68]. The curve pattern of Th/U ratios decreases from the lower to the upper section, as shown in Table 3 and Figure 2, indicating that the sedimentary rate decreases toward the upper part of the section.

### 5.1.5. Hydrothermal Activity

The ratios of (Fe + Mn)/Ti are efficient indicators for tracing hydrothermal activities. When this ratio is more than 20 ± 5 indicates that the sediments were affected by hydrothermal activity [69]. As shown in Fig. 2 and Table 3, the (Fe + Mn)/Ti ratios of samples Har 4 and Har 11 are 55 and 28, respectively, which may indicate hydrothermal activity during the Harur Formation's deposition. The occurrence of nacrite and dickite, whether associated with pyrophyllite or not, signifies the existence of hydrothermal activity [70, 71]. Mineralogical study reveals the presence of nacrite which reaches a higher amount (4.4 % in Har 11), (Table 1). The area of study as noted previously was affected by tectonic and hydrothermal activities during the Late Devonian-Early Carboniferous period.

## 6. Conclusions

Geochemical and mineralogical investigations of the early Carboniferous Harur Formation from the Ora section of northern Iraq were conducted to constrain paleoenvironmental conditions including; paleoclimate, paleoredox conditions, paleoproductivity, terrigenous clastic input, and hydrothermal activity. The paleoclimate proxies such as the CIA, A-CN-K plot, Sr/Cu ratio and binary plot of Ga/Rb versus Sr/Cu ratio, as well as the SEM result, indicate that deposition occurred primarily in a warm-humid climate with moderate to intense chemical weathering. Furthermore, lower Rb/K and Sr/Ba ratios indicate deposition in freshwater conditions and a humid climate. These may coincide with the global Devonian-early Carboniferous paleoclimate. Paleo-redox trace elements indicators like V/(V+Ni), Th/U ratios, and the U index suggest deposition under anoxic marine conditions. Paleoproductivity proxies such as the P/Ti and Ba/Al ratios, as well as their weak correlation with TOC, suggest that productivity plays a relatively minor role in organic matter accumulation. The presence of aluminium and titanium elements, quartz, clay minerals, feldspars, goethite and anatase indicate terrigenous clastic fluxes to the depositional area. Al and Ti curves generally exhibit decreasing trends from the lower to the upper part of the section suggesting that sea-level rise may be due to subsidence and/or transgression. Th/U ratios exhibit a decreasing trend from the lower to the upper section, indicating that the sedimentary rate decreases toward the upper part of the section. In addition, the positive correlation between Al and Ti with TOC reveals that clastic input plays a major role in OM accumulation, while the Ti/Al ratio indicates that grain size has a minor effect on OM distribution. The high ratios of (Fe + Mn)/Ti and the presence of nacrite minerals indicate hydrothermal activity during deposition.

**Acknowledgement:** The authors are very grateful to the College of Science, the University of Mosul for their provided facilities, which helped to improve the quality of this work. Thanks also are due to Premier OilField Group Laboratory in Houston, USA. for the great support in mineralogical and geochemical, XRD and XRF analyses and to the Department of Earth Sciences, Royal Holloway, University of London, UK for support in SEM analysis.

### References

**[1]** G. Gao, A. Titi, and S.R. Yang, "Geochemistry and depositional environment of fresh lacustrine source rock: a case study from the Triassic Baijiantan Formation shales in Junggar Basin, northwest China", *Organic Geochemistry*, vol. 113, pp. 75–89, 2017.

**[2]** M. Ivanic, G. Lojen, and J.I. Dino, "Geochemistry of sedimentary organic matter and trace elements in modern lake sediments from transitional karstic land-sea environment of the Neretva River delta (Kuti Lake, Croatia)", *Quaternary International*, vol. 494, pp. 286–299, 2017.

**[3]** J.W. Qin, S.Q. Wang, and H. Sanei, "Revelation of organic matter sources and sedimentary environment characteristics for shale gas formation by petrographic analysis of middle Jurassic

Dameigou Formation, northern Qaidam Basin, China", *International Journal of Coal Geology*, vol. 195, pp. 373–185, 2018.

**[4]** D. B. Akkoca, K.K., Eriş, M.N., Çağatay, D.B. Tekin "The mineralogical and geochemical composi-tion of Holocene sediments from Lake Hazar, Elazığ, Eastern Turkey: implications for weathering, paleo-climate, redox conditions, provenance, and tectonic setting". *Turkish Journal of Earth Sciences*, vol. 28, pp.760-785, 2019

**[5]** D. B., Akkoca, and O. Karatas ¸, "The geochemical composition of the Palu Formationfrom the Palu-Uluova basin, Elazi ğ, Eastern Anatolia (Turkey): implication of source area, weathering, and tectonic setting". *Journal of African Earth Sciences*. vol. 151, 472–489. https://doi.org/10.1016/j.jafrearsci.2019.01.007, 2019.

**[6]** M. Al-Obaiid, M.T. Ahmed, K. Khwedim, and S.A. Hussain, "Paleoredox and environmental conditions of southern Neo-Tethys deposits in south Iraq (Yamama Formation) by geochemical indicators", *Iraqi Journal of Science*, vol. 60(10), pp. 2619-2627, 2020.

**[7]** X. Zuo, C. Li, J. Zhang, G. Ma, and P. Chen, "Geochemical characteristics and depositional environment of the Shahejie Formation in Binnan oilfield, China". *Journal of Geophysical Engineering*, vol. 17, pp. 539–551, 2020.

**[8]** J.R. Hatch, and J.S. Leventhal, "Relationship between inferred redox potential of the depositional environment and geochemistry of the Upper Pennsylvanian (Missourian) Stark Shale Member of the Dennis Limestone, Wabaunsee County, Kansas, USA". *Chemical Geology*, vol. 99(1–3), pp. 65–82, 1992.

**[9]** B. Jones, and D. A. C. Manning, "Comparison of geochemical indices used for the interpretation of palaeoredox conditions in ancient mudstones". *Chemical Geology*, vol. 111, pp. 111−129, 1994.

**[10]** S.M. Rimmer, "Geochemical paleoredox indicators in Devonian-Mississippian black shales, central Appalachian Basin (USA)". *Chemical Geology*, vol. 206, 373–391, 2004.

**[11]** N. Tribovillard, T.W. Algeo, T. Lyons, and A. Riboulleau, "Trace metals as paleoredox and paleoproductivity proxies: An update". *Chemical Geology*, vol. 232, 12–32, 2006.

**[12]** A.H. Al-Hadidy, Paleozoic stratigraphic lexicon and hydrocarbon habitat of Iraq. *GeoArabia*, Gulf PetroLink, Bahrain, vol. 12(1), pp. 63−130, 2007.

**[13]** A.A. Aqrawi, J.C. Goff, A.D. Horbury, and F.N. Sadooni, *The Petroleum Geology of Iraq*. Scientific Press, Beaconsfield, United Kingdom, 2010, p. 424.

**[14]** R.A, Abdula, R. Akram, W.J. Mamaseni, F. Albeyati, "Efficiency of oil and gas generation of Palaeozoic formations outcrops in Nazdur area, Kurdistan region, Northern Iraq: insights from palynological study". *Iraqi Geological Journal*, vol. 53(1A), pp. 16–35, 2020.

**[15]** P.R. Sharland, R. Archer, D.M. Casey, R.B. Davies, S.H. Hall, A.P. Heward, A.D. Horbury, and M.D. Simmons, *Arabian Plate sequence stratigraphy*. GeoArabia, Special Publication 2, Bahrain, 2001, p. 371.

**[16]** S.Z. Jassim, and J.C. Goff, *Geology of Iraq.* Dolin, Prague and Moravian Museum, Brno, Czech Republic, 2006, p. 341.

**[17]** Z.R. Beydoun, "Arabian Plate Hydrocarbon Geology and Potential – A Plate Tectonic Approach. AAPG Studies in Geology Tulsa"*: American Association of Petroleum Geologists*, 33, 1991.

**[18]** A.I. Al-Juboury, and A.H. Al-Hadidy, "Facies and depositional environments of the Devonian-Carboniferous succession of Iraq". *Geological Journal*, 4 vol. 3, pp. 383−396, 2008.

**[19]** A.I. Al-Juboury, and A.H. Al-Hadidy, "Petrology and depositional evolution of the Paleozoic rocks of Iraq". *Marine and Petroleum Geology*, vol. 26, pp. 208−231, 2009.

**[20] [20]** A.I. Al-Juboury, A combined petrological-geochemical study of the Paleozoic successions of Iraq. In: A.H. Al-Juboury, (Ed.), *Petrology-new perspectives and applications*, InTech Publishing, Croatia, pp. 169-199, 2012.

**[21]** J. Gaddo, and D.M.F. Parker, Final report on well Khlesia No. 1: MPC Report, no. FWR 28, INOC Library, Baghdad, 1959.

**[22]** Y.K. Al-Haba, F.H. Khalaf, M. Al-Rabaii, and A. Michal, Regional geology studies for Paleozoic section, west Iraq. EOC unpublished report, Baghdad, Iraq, 1991.

**[23]** Y.K. Al-Haba, A. Al-Samarrai, F. Al-Jboury, N.N. Georgis, and I.M. Ahmed, Exploration for the Paleozoic prospects in western Iraq, part 1: exploration of the Paleozoic system in western Iraq, Proceedings of the second seminar on hydrocarbon potential of deep formation in the Arab countries (OAPEC), Cairo 10-13 October, pp. 1−21. (in Arabic), 1994.

**[24]** A.H. Al-Hadidy, *Facies and Sedimentary Environment of Late Paleozoic Successions (Devonian–Permian) of Iraq*. Unpublished PhD Thesis, Mosul University, Iraq, 2001.
**[25]** R.C. Bellen, van, H.V. Dunnington, W. Wetzel, and D.M. Morton, *Lexique Stratigraphique International*, Asie, Fasc. 10a, Iraq. Centre Natl. Rech. Scii., Paris, 1959, p. 333.
**[26]** T. Buday, *The Regional Geology of Iraq, v. 1, Stratigraphy and Paleogeography*. Dar Al-Kutub Publishing House, University of Mosul, Mosul, Iraq, 1980, p. 445.
**[27]** G.H. Shirwani, S.F. Naqishbandi, and S.M. Balaky, "Microfacies and Environmental Analysis of Harur Formation Early Carboniferous (Tournaisian) Northern Iraqi Kurdistan Region". *Iraqi Bulletin of Geology and Mining*, vol. 2, pp. 239–255, 2006.
**[28]** V.K. Sissakian, Geological Map of Iraq, scale 1: 1 000 000, 3rd edit. GEOSURV, Baghdad, Iraq, 2000.
**[29]** M.M. Herron, "Geochemical classification of terrigenous sands and shales from core or log data". *Journal of Sedimentary Research*, vol. 58 (5), pp. 820–829, 1988.
**[30]** S.R. Taylor, and S.M. McLennan, *The Continental Crust: Its Composition and Evolution*. Blackwell, Oxford, 1985, p. 312.
**[31]** H.W. Nesbitt, and G.M. Young, "Early Proterozoic climates and plate motions inferred from major element chemistry of lutites". *Nature*, vol. 299, pp. 715–717, 1982.
**[32]** P. Wang, Y. Du, W. Yu, T.J. Algeo, Q. Zhou, Y. Xu, L. Qi, L. Yuan, and W. Pan, "The chemical index of alteration (CIA) as a proxy for climate change during glacial-interglacial transitions in Earth history". *Earth Science Review*, vol. 201, 103032, 2020.
**[33]** S.M. McLennan, S. Hemming, D.K. McDaniel, and G.N. Hanson, Geochemical approaches to sedimentation, provenance and tectonics. In: J.M. Johnsson, and A. Basu, (Eds.) *Processes controlling the composition of clastic sediments. Geological Society of America Special Paper*, pp. 21–40, 1993.
**[34]** F.H. Tobia, H. S. Al-Jaleel, and I. N. Ahmad, "Provenance and depositional environment of the Middle-Late Jurassic shales, northern Iraq", *Geosciences Journal*, vol. 25(3), doi.org/10.1007/s12303-018-0072-62019.
**[35]** J. Ding, J. Zhang, X. Tang, Z. Huo, S. Han, L. Yue, Y. Zheng, L. Xingqi, T. Liu, "Elemental Geochemical Evidence for Depositional Conditions and Organic Matter Enrichment of Black Rock Series Strata in an Inter-Platform Basin: The Lower Carboniferous Datang Formation, Southern Guizhou, Southwest China". *Minerals*, vol. 8 (11), 509; 2018. https://doi.org/10.3390/min8110509.
**[36]** Y. Liu, Ch. Song, Q. Meng, P. He, R. Yang, R. Huang, S. Chen, D. Wang, and Z. Xing, "Paleoclimate change since the Miocene inferred from clay-mineral records of the Jiuquan Basin, NW China". *Palaeogeography, Palaeoclimatology, Palaeoecology*, vol. 550, 109730, 2020.
**[37]** H. Chamley, Clay Sedimentology. Springer-Verlag, Berlin, 1989, p. 623.
**[38]** A. I. Al-Juboury, M. A. Al-Haj, A. Hutton and B. Jones, "Clay minerals and organic matter from deeply buried Ordovician-Silurian shale in western Iraq: implications for maturity and hydrocarbon generation", *Iraqi Journal of Science*, vol. 61 (11), pp. 3006-3023, 2020.
**[39]** S. H. Hussain, A. I. Al-Juboury, M.A. Al-Haj, J. S. Armstrong-Altrin and S. F. Al-Lhaebi, "Mineralogy and geochemistry of the Late Triassic Baluti Formation, Northern Iraq", *Journal of African Earth Sciences*, vol. 181, https://doi.org/10.1016/j.jafrearsci.2021.104243, 2021.
**[40]** Z. Zhen, W. Li, L. Xu, C. Wang, and L. Zhao, "Characteristics of palaeosalinity and palaeoredox records in sediment from Dali Lake: Climate change in North China from 0 to 2100 cal BP". *Quaternary Geochronology*, vol. 60, 101104, 2020.
**[41]** L. Li, Z. Liu, P. Sun, Y. Li, and S.C. George, "Sedimentary basin evolution, gravity flows, volcanism, and their impacts on the formation of the Lower Cretaceous oil shales in the Chaoyang Basin, northeastern China". *Marine and Petroleum Geology*, vol. 119, 104472, 2020.
**[42]** T.J. Algeo, and J.B. Maynard, "Trace-element behavior and redox facies in core shales of Upper Pennsylvanian Kansas-type cyclothems". *Chemical Geology*, vol. 206, pp. 289–318, 2004.
**[43]** P.B. Wignall, and R.J. Twitchett, "Oceanic anoxia and the end Permian mass extinction". *Science*, vol. 272, pp. 1155-1158, 1996.
**[44]** M. Steiner, E. Wallis, B.D. Erdtmann, Y. Zhao, and R. Yang, "Submarine-hydrothermal exhalative ore layers in black shales from South China and associated fossils-insights into a Lower Cambrian facies and bioevolution". *Palaeogeography Palaeoclimatology Palaeoecology*, vol. 169, pp. 165–191, 2001.

**[45]** H.J. Brumsack, "The trace metal content of recent organic carbon-rich sediments: implications for Cretaceous black shale formation". *Palaeogeography Palaeoclimatology Palaeoecology*, vol. 232, pp. 344–361, 2006.
**[46]** J. Shen, S. Schoepfer, Q.L. Feng, L. Zhou, J.X. Yu, H.Y. Song, H.Y. Wei, and T.J. Algeo, "Marine productivity changes during the End-Permian crisis and Early Triassic recovery". *Earth Science Review*, vol. 149, pp. 136–162, 2015.
**[47]** J. Dymond, E. Suess, and M. Lyle, "Barium in deep-sea sediment: a geochemical proxy for paleoproductivity". *Paleoceanography*, vol. 7(2), pp. 163–181, 1992.
**[48]** A. Paytan, M. Kastner, and F.P. Chavez, "Glacial to interglacial fluctuations in productivity in the equatorial Pacific as indicated by marine barite". *Science*, vol. 274 (5291), pp. 1355–1357, 1996.
**[49]** B. Xiao, S.G. Liu, B. Ran, and Z.W. Li, "Geochemistry and sedimentology of the Upper Ordovician–lower Silurian black shale in the northern margin of the Upper YangtzePlatform, South China: implications for depositional controls on organic-matter accumulation". *Australian Journal of Earth Science*, vol. 67 (1), pp. 129–150, 2020.
**[50]** W.E. Dean, J.V. Gardner, and D.Z. Piper, "Inorganic geochemical indicators of glacial-interglacial changes in productivity and anoxia on the California continental margin". *Geochimica et Cosmochimica Acta*, vol. 61 (21), pp. 4507–4518, 1997.
**[51]** M. Reolid, F.J. Rodriguez-Tovar, A. Marok, and A. Sebane, "The Toarcian oceanic anoxic event in the Western Saharan Atlas, Algeria (North African paleomargin): Role of anoxia and productivity". *Geological Society American Bulletin*, vol. 124, pp. 1646–1664, 2012.
**[52]** Y. Lu, S. Jiang, Y. Lu, S. Xu, Y. Shu, and Y. Wang, "Productivity or preservation? The factors controlling the organic matter accumulation in the late Katian through Hirnantian Wufeng organic-rich shale, South China". *Marine and Petroleum Geology*, vol. 109, pp. 22–35, 2019.
**[53]** S. Yang, W. Hu, S. Yao, X. Wang, W. He, Y. Wang, and F. Sun, "Constraints on the accumulation of organic matter in Upper Ordovician-lower Silurian black shales from the Lower Yangtze region, South China". *Marine and Petroleum Geology*, vol. 120, 104544, 2020.
**[54]** C. Jin, Z. Liao, and Y. Tang, "Sea-level changes control organic matter accumulation in the Longmaxi shales of southeastern Chongqing, China". *Marine and Petroleum Geology*, vol. 119, 104478, 2020.
**[55]** D.A. Timothy, and S.E. Calvert, "Systematics of variations in excess Al and Al/Ti in sediments from the central equatorial Pacific". *Paleoceanography*, vol. 13(2), pp. 127–130, 1998.
**[56]** Y. Liu, B. Wu, Q. Gong, and H. Cao, "Geochemical characteristics of the lower Silurian Longmaxi Formation on the Yangtze Platform, South China: Implications for depositional environment and accumulation of organic matters". *Journal of Asian Earth Science*, vol. 184, 104003, 2019.
**[57]** G.D. Sharma, *The Alaskan Shelf Hydrographic, Sedimentary and Geochemical Environment.* Springer-Verlag, New York, 1979, p. 498.
**[58]** E.T. Degens, *Geochemistry of sediments: A brief survey.* Prentice-hall, New Jersey, 1965, p. 369.
**[59]** M.A. Arthur, and B.B. Sageman, "Marine black shales e depositional mechanisms and environments of ancient deposits". *Annual Review Earth Planetary Sciences*, vol. 22, pp. 499–551, 1994.
**[60]** L.E.J. Ibach, "Relationship between sedimentation rate and total organic carbon content in ancient marine sediments". *American Association of Petroleum Geologists Bulletin*, vol. 66, pp. 170–188, 1982.
**[61]** S.M. Rimmer, J.A. Thompson, S.A. Goodnight, and T.L. Robl, "Multiple controls on the preservation of organic matter in Devonian-Mississippian marine black shales: geochemical and petrographic evidence". *Palaeogeography Palaeoclimatology Palaeoecology*, vol. 215, pp. 125–154, 2004.
**[62]** S. Duggen, P. Croot, U. Schacht, and L. Hoffmann, "Subduction zone volcanic ash can fertilize the surface ocean and stimulate phytoplankton growth: Evidence from biogeochemical experiments and satellite data". *Geophysical research letters*, vol. 34 (1), 2007.
**[63]** C.R. Hamme, W.P. Webley, R.W. Crawford, A.F. Whitney, D.M. DeGrandpre, R.S. Emerson, C.C. Eriksen, E.K. Giesbrecht, F.R.J. Gower, T.M. Kavanaugh, M. Angelica Peña, L.C. Sabine, D.S. Batten, A.L. Coogan, and S.D. Grundle, "Volcanic ash fuels anomalous plankton bloom in subarctic northeast Pacific". *Geophysical Research Letters*, vol. 37, L19604, 2010. http://dx.doi.org/10.1029/2010GL044629.

**[64]** J. Olsson, S.L.S. Stipp, K.N. Dalby, and S.R. Gislason, "Rapid release of metal salts and nutrients from the 2011 Grímsvötn, Iceland volcanic ash". *Geochimica et Cosmochimica Acta*, vol. 123, pp. 134–149, 2013.

**[65]** J.I. Hedges, and R.G. Keil, "Sedimentary organic matter preservation: an assessment and speculative synthesis". *Marine Chemistry*, vol. 49, pp. 123–126, 1995.

**[66]** P. Bertrand, G. Shimmield, P. Martinez, F. Grousset, F. Jorissen, C.J. Pujol, I. Bouloubassi, P. Buat Menard, J.P. Peypouquet, L. Beaufort, M.A. Sicre, E. Lallier-Verges, J.M. Foster, and Y. Ternois, "The glacial ocean productivity hypothesis: the importance of regional temporal and spatial studies". *Marine Geology*, vol. 130 (1-2), pp. 1–9, 1996.

**[67]** A.E. Murphy, B.B. Sageman, D.J. Hollander, T.W. Lyons, and C.E. Brett, "Black shale deposition in the Devonian Appalachian Basin: siliciclastic starvation, episodic water-column mixing, and efficient recycling of bio limiting nutrients". *Paleoceanography*, vol. 15, pp. 280–291, 2000.

**[68]** F. Goodarzi, T. Gentzis, H. Sanei, and P.K. Pedersen, "Elemental composition and organic petrology of a Lower Carboniferous-age freshwater oil shale in Nova Scotia, Canada". *ACS Omega*, vil. 4, 20773−20786, 2019.

**[69]** C.L. Chu, Q.L. Chen, B. Zhang, Z. Shi, H.J. Jiang, and X. Yang, "Influence on Formation of Yuertusi Source Rock by Hydrothermal Activities at Dongergou Section, Tarim Basin". *Acta Sedimentologica Sinica*, vol. 34, pp. 803–810. (in Chinese with English abstract), 2016.

**[70]** C.O. Choo, and S.J. Kim, "Dickite and other kaolin polymorphs from an Al-rich kaolin deposit formed in volcanic tuff, southeastern Korea". *Clays and Clay Minerals*, vol. 52 (6), pp. 749–759, 2004.

**[71]** A. Gaudin, V. Ansan, J.P. Lorand, and S. Pont, "Genesis of a florencite-bearing kaolin deposit on ordovician schists at Saint-Aubin-des-Châteaux, Armorican Massif, France". *Ore Geology Reviews*, vol. 120, 103445, 2020.